Biochemical Pharmacology, Vol. 58, pp. 95–107, 1999.

ISSN 0006-2952/99/$–see front matter
PII S0006-2952(99)00083-0

Cell Cycle-Dependent Distribution and Specific Inhibitory Effect of Vectorized Antisense Oligonucleotides in Cell Culture

Valérie Hélin,§ Marina Gottikh,*† Zohar Mishal,‡ Frédéric Subra,* Claude Malvy* and Marc Lavignon**

*Laboratoire de Biochimie-Enzymologie, UMR 8532, Institut Gustave-Roussy, 94800 Villejuif, France; †Belozersky Institute of Physico-Chemical Biology, Lomonosov Moscow State University, 117899 Moscow, Russia; and ‡CNRS IFC-01, Laboratoire de cytometrie, 94800 Villejuif, France

ABSTRACT. Factors limiting the use of antisense phosphodiester oligodeoxynucleotides (ODNs) as therapeutic agents are inefficient cellular uptake and intracellular transport to RNA target. To overcome these obstacles, ODN carriers have been developed, but the intracellular fate of ODNs is controversial and strongly depends on the means of vectorization. Polyamidoamine dendrimers are non-linear polycationic cascade polymers that are able to bind ODNs electrostatically. These complexes have been demonstrated to protect phosphodiester ODNs from nuclease degradation and also to increase their cellular uptake and pharmacological effectiveness. We studied the intracellular distribution of a fluorescein isothiocyanate-labeled ODN vectorized by a dendrimer vector and found that intracellular ODN distribution was dependent on the phase of the cell cycle, with a nuclear localization predominantly in the G2/M phase. In addition, in order to evaluate the relevance of ODN vectors in enhancing the inhibition of the targeted genes' expression, we developed a rapid screening system which measures the transient expression of two reporter genes, one used as target, the other as control and vice versa. This system was validated through investigating the effect of the dendrimer vector on ODN biological activity. Antisense sequence-specific inhibition of more than 70% of one reporter gene was obtained with a chimeric ODN containing four phosphorothioate groups, two at each end. BIOCHEM PHARMACOL **58**;1:95–107, 1999. © 1999 Elsevier Science Inc.

KEY WORDS. antisense oligodeoxynucleotide; polyamidoamine dendrimer; intracellular distribution; cell cycle, screening system

ODNs‖ are being increasingly used as potential therapeutic agents in clinical trials [1, 2]. Promising results have been reported, particularly for the treatment of malignant cells [3–5] and cells infected by viruses [6–8]. However, the problems related to ODN stability in biological media and their cellular uptake and transport to RNA targets have not been completely resolved. Chemical modifications, especially in the phosphodiester ODN backbone, have been performed to increase both ODN resistance to nucleases and cellular uptake [9–11]. The phosphorothioate ODNs, in which one non-bonding oxygen is replaced by a sulphur atom, are the molecules most often employed as antisense ODNs. However, these resistant analogs pose problems such as chirality and non-sequence-specific effects [12]. Vectorizing ODNs is a complementary approach aimed at enhancing their efficiency. ODNs have been conjugated with a wide series of molecules (e.g. cholesterol [13–15], acridine [16], fusogenic peptide [17, 18]), encapsulated within liposomes [19, 20] and immunoliposomes [21, 22], and adsorbed on nanoparticles [23, 24], all of which have yielded interesting results. ODNs have been demonstrated to be protected against nuclease degradation when complexed to poly-L-lysine [25] or cationic lipids [26–28]. Although some of these compounds raise problems specifically related to stability in biological media and cellular toxicity, certain molecules are promising and may ultimately be used *in vivo* [29–31].

Among the candidates considered eligible for vectorization of ODNs, dendrimeric structures have great potential. Polyamidoamine dendrimers were first developed as new delivery agents for DNA transfections [32]. They have a spherical architecture with branches radiating from a central core and terminating in charged amino groups. This structure is able to complex nucleic acids, through electrostatic interactions, and to act as a buffer in the endosomal

§ Corresponding author: Valérie Hélin, Institut Gustave Roussy, CNRS UMR 8532, 39 Rue Camille Desmoulins, 94800 Villejuif, France. Tel. 33 01 42 11 54 02; FAX: 33 01 42 11 52 76; E-mail: vhelin@igr.fr.

‖ *Abbreviations:* AUG-ODNs, ODNs complementary to the initiation codon of the targeted gene; β-gal, β-galactosidase protein; CPRG, chlorophenolred-β-D-galactopyranoside; DMEM, Dulbecco's modified Eagle's medium; FBS, fetal bovine serum; FITC, fluorescein isothiocyanate; GFP, green fluorescent protein; IN-ODNs, ODNs complementary to an internal region of the targeted gene; MTT, 3-[4,5-dimethylthiazol-2-yl]-2,5-diphenyltetrazolium bromide; and ODN, oligodeoxynucleotide.

Received 3 September 1998; accepted 12 January 1999.

TABLE 1. ODN sequences used for biological assays

ODN	Length	Sequence	Target	Position*
AUG-β-gal	18-mer	$T_{(S)}A_{(S)}A$ ACG ACA TGG TGA $C_{(S)}T_{(S)}T$	initiation codon β-gal	865–882
IN-β-gal	18-mer	$T_{(S)}G_{(S)}G$ TAG CGA CCG GCG $C_{(S)}T_{(S)}C$	internal coding region β-gal	3971–3988
AUG-GFP	18-mer	$T_{(S)}G_{(S)}C$ TCA CCA TGG TGG $C_{(S)}G_{(S)}A$	initiation codon EGFP-N1	671–688
IN-GFP† antisense	18-mer	$G_{(S)}A_{(S)}G$ CTG CAC GCT GCC $G_{(S)}T_{(S)}C$	internal coding region EGFP-N1	1198–1215
Control	21-mer	$T_{(S)}G_{(S)}A$ ACA CGC CAT GTC GAT $T_{(S)}C_{(S)}T$	non-complementary to both plasmids	
IN-GFP reverse	18-mer	$C_{(S)}T_{(S)}G$ CCG TCG CAC GTC $G_{(S)}A_{(S)}G$		
IN-GFP scramble	18-mer	$T_{(S)}C_{(S)}C$ GCC CTG AGC TGA $G_{(S)}C_{(S)}G$		
IN-GFP double mismatch	18-mer	$G_{(S)}A_{(S)}G$ CT<u>C</u> CAC GC<u>A</u> GCC $G_{(S)}T_{(S)}C$		

*The positions indicated correspond to the sequences targeted in the pCMVβ-gal and pEGFP-N1 plasmids.
†This ODN sequence was also used for flow cytometry and confocal microscopy analysis with a phosphodiester analog containing an FITC group at each end.

compartment once inside cells [33]. Results obtained with such complexes have shown that they protect phosphodiester ODNs from nuclease degradation [33], improve the cellular uptake of antisense ODNs [34, 35], and facilitate inhibition of the expression of specific genes [36, 37]. Moreover, compared to many other ODN carriers, dendrimeric structures offer significant advantages such as excellent reproducibility, weak cytotoxicity, and rapid complex formation [33, 35]. In this study we have investigated, by flow cytometry and confocal microscopy analyses, the effect of a dendrimeric structure (SuperFect™) on the uptake and intracellular distribution of a 3′ and 5′ labeled FITC–ODN as a function of cell cycle phase.

In addition, the search for further chemical modifications and/or new vectors able to increase the biological activity of ODNs is often hampered by the absence of a rapid assay system. We have developed a rapid screening system using two reporter genes under the control of the same promoter to identify the biological activity of vectorized ODNs. One of the most interesting features of this system is its ability to measure the inhibition of one gene's expression using another gene as a control for cytotoxic and non-sequence-specific effects. The effectiveness of the dendrimer in enhancing the biological activity of antisense ODNs was tested using this screening system. An antisense sequence-specific inhibition of 76% was obtained for one reporter gene with a chimeric ODN containing four phosphorothioate groups, two at each end.

MATERIALS AND METHODS

Chemical and Transfecting Reagents

Ethylenediamine dihydrochloride, 1-ethyl-3(3′-dimethylaminopropyl)carbodiimide, FITC isomer I, Hoechst 33342, thymidine, 2′-deoxycytidine, and MTT (thiazolyl blue) were purchased from Sigma. 5′-Phosphate-ON™ was purchased from Clontech. Propidium iodide and CPRG were purchased from Boehringer Mannheim. SuperFect™ (3 mg/mL) was purchased from Qiagen.

Cells and Media

HeLa (human epitheloid carcinoma cells; F. Clavel, Institut Pasteur, Paris, France) and NIH 3T3 (murine fibroblast cells; F. Dautry, CNRS, Villejuif, France) cell lines were grown in DMEM medium supplemented, respectively, with 10% and 5% of heat-inactivated FBS (GIBCO BRL), streptomycin (100 μg/mL), and penicillin (100 U/mL). The CEM-4 cell line (human T cells; A. M. Aubertin, CNRS, Strasbourg, France) was maintained in RPMI 1640 with 10% of decomplemented FBS and antibiotics. All cell lines were incubated at 37° in 5% CO_2. The culture media, trypsin, and PBS were pre-warmed to 37° before adding on cells.

Plasmids and Oligonucleotides

The pCMVβ-gal and pEGFP-N1 plasmids were purchased from Clontech. The β-actin plasmid (pBACT5) was a generous gift from Dr. F. Dautry (CNRS, Villejuif, France). The ODNs with two phosphorothioate bonds at the 5′ and 3′ ends were synthesized and purified by Eurogentec (see Table 1 for ODN sequences).

Synthesis and Purification of FITC–ODN

An oligonucleotide (IN-GFP antisense phosphodiester analog) with a phosphate flanking the 5′ and 3′ ends was synthesized using the routine β-cyanoethyl phosphoramide method and 5′-phosphate-ON™ as the phosphorylating agent. A solution containing the 3′-5′-phophorylated oligonucleotide (0.1–0.2 μmol) in 700 μL of water was supplemented with 240 mg of ethylenediamine dihydrochloride (1.8 mmol) and 120 mg of 1-ethyl-3(3′-dimethylaminopropyl) carbodiimide (0.6 mmol). The mixture was vortexed and incubated at room temperature for 3 hr. The oligonucleotide ethylenediamine derivative was then separated from excess reagents by size exclusion on a NAP-10 column (Pharmacia LKB Biotechnology), followed by precipitation by adding a 10-fold excess of 2% $LiClO_4$ in acetone. Subsequently, this derivative was dissolved in 60 μL of water and the solution was supplemented with 20 μL

of 1 M carbonate buffer, pH 11, and 80 μL of dimethylacetamide, and then 1 mg of FITC (2.5 μmol) was added. The mixture was vortexed and incubated at room temperature in the dark for 2–4 hr. The FITC–ODN conjugate was separated from salts and free FITC by size exclusion on a NAP-10 column and purified by 20% PAGE in the presence of 7 M urea. The presence of an FITC group at the ends of the ODN was confirmed by spectrophotometer measurement. The ratio between the extinction of FITC at 490 nm and total extinction of FITC–ODN at 260 nm corresponded to the presence of approximately two fluorescein residues to one ODN molecule.

Preparation of Plasmid and Oligonucleotide Complexed to Transfecting Reagent

For the fluorescence analysis, 5 μg of FITC–ODN was mixed with 5 μL of SuperFect™ (15 μg) in a final volume of 60 μL of DMEM (without FBS and antibiotics) for 10 min at room temperature. For the biological assay, 1.2 μg of plasmids (0.8 μg of pEGFP-N1 and 0.4 μg of pCMVβ-gal) was mixed with 6 μL of SuperFect™ (18 μg) in a final volume of 150 μL of DMEM (without FBS and antibiotics) for 10 min at room temperature. Different quantities of ODNs (0.25 to 10 μg) were complexed to 6 μL of SuperFect™ according to the same procedure. SuperFect™ is a dendrimeric structure presenting 140 terminal NH_2 groups on its surface (sixty of which are positively charged at pH 7) and with a molecular weight of 35,000. This means that, for example, with 5 μg of an 18-mer ODN, the SuperFect™/ODN charge ratio is 2/1.

Cell Transfection Protocol

The FBS used for cell transfection was always heat-inactivated for 30 min at 56°. For the fluorescence analysis, cells were seeded on 24-well plates or on Lab-Teck chambered cover glasses (4 chambers, Nunc Inc.). The following day, the 60 μL of the SuperFect™–FITC–ODN mixture was diluted with 360 μL of 5% or 10% FBS in DMEM (for HeLa and NIH 3T3 cells, respectively) and added to cells, previously washed with PBS. For the biological assay, cells were seeded on 6-well plates to obtain 60–80% confluency (4.10^5 HeLa cells). The next day, cells were washed with PBS and treated with the 150 μL of the SuperFect™–ODN preparation diluted with 700 μL of 10% FBS DMEM (with antibiotics), 2 hr before the addition of the 150 μL of SuperFect™–plasmid mixture.

Flow Cytometry Analysis

For the flow cytometry analysis, cells were seeded on 24-well plates (8.10^4 HeLa and CEM-4 cells, 4.10^4 NIH 3T3 cells). The following day, 5 μg of FITC–ODN complexed to SuperFect™ was incubated with cells for different times. Adherent cells were trypsinized and then all cells were washed with PBS. Cells were centrifuged for 10 min at 400 *g* and resuspended in 400 μL of PBS containing 10 μg/mL propidium iodide. Mean cellular fluorescence intensities for 5,000 or 10,000 viable cells (2,000 for CEM cells) were determined on a Coulter EPICS Elite dual-laser flow cytometer. Dead cells were excluded by two means: through forward and side scatter gatings and by using propidium iodide to stain the dead cells. For cell cycle measurements, cells were resuspended in PBS containing 10 μg/mL propidium iodide and 20 μg/mL Hoechst 33342, incubated in the dark for 30 min at 37° [38] and analyzed by dual-laser flow cytometer. The cell cycles were obtained using the advanced version of the Multicycle AV program developed by P. Rabinovich (Seattle, WA, U.S.A.) and distributed by Phoenix Flow Systems.

Confocal Microscopy Analysis

A Meridian ACAS 570 (Meridian Instruments), fitted with an argon–ion laser and an Olympus IMT-2 inverted microscope, was used for microscopy analysis. Excitation was performed at 488 nm and the filter combination used to detect emission was that conventionally used for fluorescein. The pinhole was set either at 225 or 400 (range of 40–1600) and the photomultiplier voltage at 25% for optimal resolution. Cells were plated on Lab-Teck chambered cover glasses (4 chambers) (5.10^4 HeLa cells and 2.10^4 NIH 3T3 cells). The following day, FITC–ODN complexed to SuperFect™ was added as previously described. After different times of incubation, cells were washed twice with PBS, and 400 μL of fresh medium was added. Confocal microscopy analysis was then carried out after incubating cells for different times in fresh medium.

FITC-ODN Stability Inside Cells

FITC–ODN (5 μg) delivered by SuperFect™ was incubated for 16 hr with HeLa cells in a 12-well plate. Cells were washed three times with PBS, trypsinized, centrifuged, and washed again three times with PBS. The pellet was resuspended in 1 mL of water, vortexed, and kept for 30 min at −20°. FITC–ODN was then isolated by phenol extraction, precipitated by adding a 10-fold excess of 2% $LiClO_4$ in acetone, and analyzed by 20% PAGE containing 7 M urea. The gel was read using a fluoroimager (Storm 840, Molecular Dynamics).

Cell Synchronization

HeLa cells were synchronized using the double thymidine block procedure [39]. Cells were seeded on 24-well plates for flow cytometry analysis (8.10^4 cells) and on Lab-Teck cover glass chambers (4 chambers) for flow cytometry and confocal microscopy analysis in parallel (4.10^4 cells). A first thymidine block was imposed by removing the growth medium and providing fresh medium containing 2 mM

thymidine. Cells were blocked for 16 hr and released from the first block by washing with serum-free medium before the medium was replaced with normal growth medium containing 24 μM deoxycytidine for 9 hr. A second thymidine block was imposed by adding serum-free medium containing 2 mM thymidine. After 16 hr, cells were released with normal fresh medium. The vectorized FITC–ODN was then added to cells at different times for 4 hr of incubation.

Biological Assay System

β-Galactosidase and green fluorescent protein [40] expression was detected 16 hr after plasmid co-transfection. Cells were washed twice with PBS, and 400 μL of reporter lysis buffer (Promega) was added for 15 min. Cells were then scraped and centrifuged at 10,000 *g* for 15 min at 4°. For the β-galactosidase assay, 5 μL of supernatant was mixed with 100 μL of a CPRG reaction buffer (4.6 mg/mL CPRG, 80 mM phosphate buffer pH 7.4, 0.7% β-mercaptoethanol and 9 mM $MgCl_2$) in a 96-well plate and incubated at 37° for 20 min. β-Galactosidase activity was then detected by reading the absorbance at 570 nm using an automatic reader spectrophotometer (Dynatech Laboratories). The amount of green fluorescent protein was directly measured on the remaining supernatant with a spectrofluorimeter (Kontron SFM 23/B) using a 488 nm excitation wavelength and reading the emission at 507 nm.

mRNA Analysis

HeLa cells were treated with ODN and plasmids as previously described. Total cellular RNA was resolved on 1% agarose gels containing 1.1% formaldehyde and transferred to nitrocellulose membranes. The blots were then hybridized overnight with a GFP DNA probe ^{32}P-radiolabeled with [α-^{32}P]dCTP by random primer labeling using a commercially available kit (Oncor-Appligene). After washing, hybridizing bands were visualized using a phosphorimager (Storm 840). The blots were then stripped of radioactivity by boiling and reprobed with a ^{32}P-labeled β-actin DNA probe to evaluate RNA loading.

Cytotoxicity Measurement

Cellular toxicity of the transfecting reagent was evaluated under the different experimental conditions using the MTT assay [41]. After washing cells with PBS, 100 μL of MTT (5 mg/mL in PBS) was added to each well. Cells were then incubated at 37° for 90 min (6-well plate) or 3 hr (24-well plate). Lysis buffer (1 mL; 10% SDS, 10 mM HCl) was then added for an overnight incubation at 37°. After that, the absorbance at 570 nm, which is directly correlated to cell viability, was read.

RESULTS

Flow Cytometry Evaluation of Uptake Efficiency and Kinetics

The ability of a dendrimeric structure (SuperFect™) to facilitate ODN uptake was first evaluated on non-synchronous murine fibroblast (NIH 3T3), human epitheloid carcinoma (HeLa), and non-adherent human T lymphocyte (CEM-4) cell lines. Mean fluorescence was measured taking into account only living cells. The flow cytometry analysis showed insignificant fluorescence when the cell lines were incubated with FITC–ODN alone. In contrast, complexation of FITC–ODN to the transfecting reagent strongly increased cellular fluorescence intensity in adherent cell lines; the number of fluorescent cells was greater in HeLa than in NIH 3T3 cells and the distribution around the mean was less broad (Fig. 1). Interestingly, a small proportion of cells exhibited a strong intensity of fluorescence, at least 10 times higher than the intensity of the majority of fluorescent cells (Fig. 1, B′). This subpopulation of intensely fluorescent cells represents 5 to 10% of the total fluorescent cell population. The kinetics of the uptake of FITC–ODN complexed to SuperFect™ was also evaluated in HeLa cells. After 30 min, fluorescent cells could already be detected. The percentage of fluorescent cells increased progressively during the first 4 hr, reaching a plateau of 80 to 90% (Fig. 2). Under our experimental conditions, the cytotoxicity of the ODN–SuperFect™ complex was found to be insignificant on HeLa cells and approximately 30% on NIH 3T3 cells.

Investigation of Intracellular Distribution by Confocal Microscopy

Flow cytometry analysis does not differentiate membrane-bound from internalized fluorescence and does not indicate precisely where fluorescence is located. The uptake analysis was therefore completed by a confocal microscopy study on non-synchronous HeLa and NIH 3T3 cells. Uptake was studied after different times of incubation (from 1 to 24 hr) with FITC–ODN complexed to the dendrimer vector. After 1 hr of incubation, ODN fluorescence was found on the cellular membrane and inside of cells (Fig. 3A), and was totally internal after 16 hr of incubation (Fig. 3B). These results strongly suggested that the fluorescence observed during flow cytometry corresponded to ODN uptake, considering that the FITC–ODN is not degraded once inside cells (see below). Moreover, with the confocal microscope, heterogeneity of the intracellular distribution of fluorescence was observed in the cell population with both adherent cell lines, whatever the time of incubation with vectorized FITC–ODN (from 1 to 24 hr). Two patterns of fluorescence were detected: some cells exhibited perinuclear fluorescence and others showed strong nuclear fluorescence (Fig. 4). The same heterogeneity of fluorescence distribution was found in cell samples incubated for 16 hr with vectorized FITC–ODN and analyzed at different times

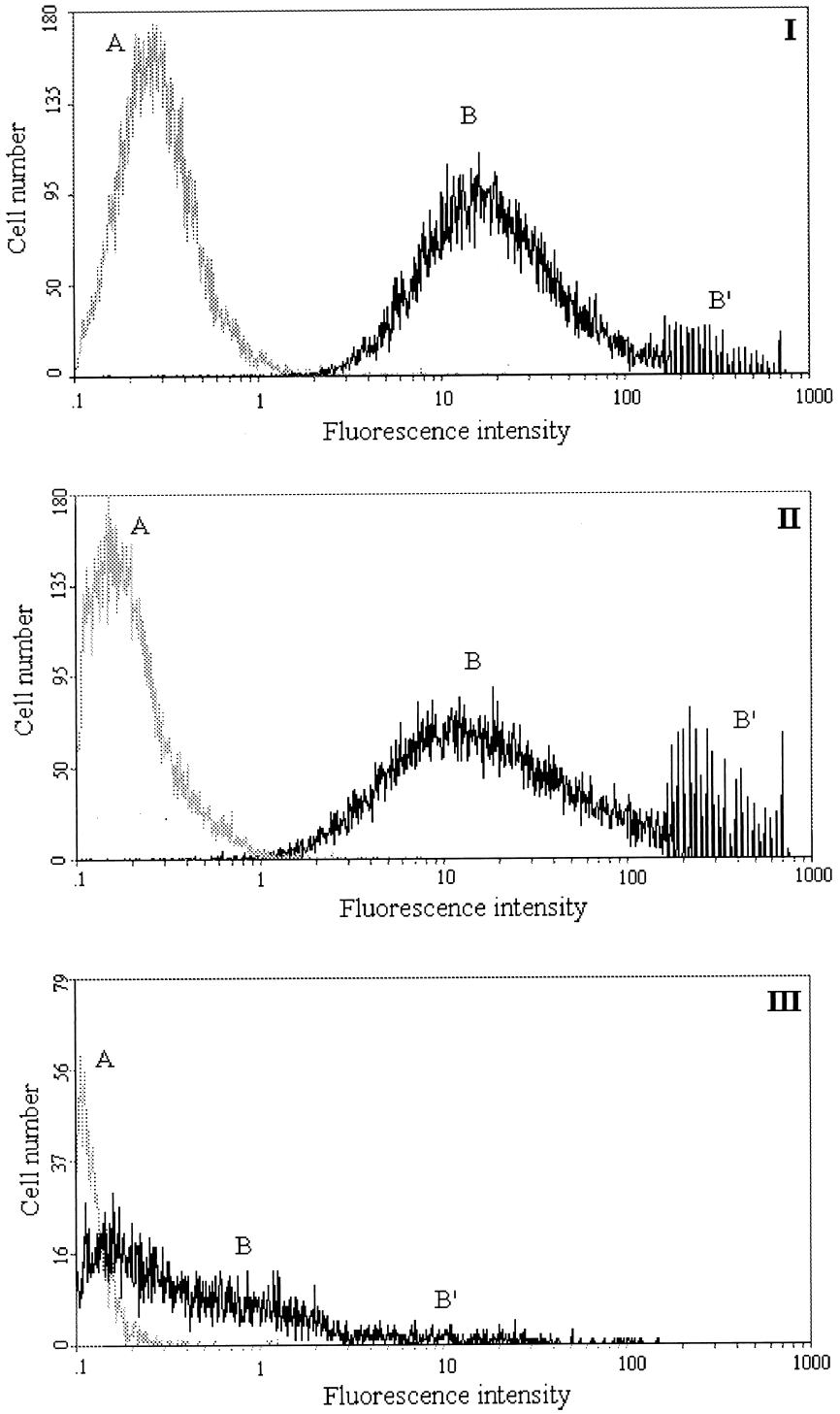

FIG. 1. Comparison of cellular fluorescence intensities. Uptake of vectorized FITC–ODN was determined after 16 hr of incubation by flow cytometry analysis. (I) HeLa cells: (A) control without FITC–ODN; (B) FITC–ODN complexed to SuperFect™. (II) NIH 3T3 cells: (A) control without FITC–ODN; (B) FITC–ODN complexed to SuperFect™. (III) CEM-4 cells: (A) control without FITC–ODN; (B) FITC–ODN complexed to SuperFect™. B′ (I, II, and III): subpopulation of fluorescent cells presenting a much higher level of fluorescence intensity.

after removal of the medium containing FITC–ODN (from 1 to 24 hr). Consequently, the two patterns of intracellular distribution of fluorescence were not dependent on the time cells were incubated with FITC–ODN or on the time following the removal of the medium with FITC–ODN. One of our hypotheses was that these two patterns of fluorescence distribution observed by confocal microscopy could be related to the difference in cellular intensity of fluorescence detected by flow cytometry (Fig. 1, B and B′).

The fact that fluorescent cells were attached and presented well-demarcated cytoplasmic and nuclear membranes, whatever the time of incubation with vectorized FITC–ODN, was strong evidence of their viability. In addition, we carried out experiments using propidium iodide, which makes it possible to distinguish dead cells, and fluorescent cells were found not to be stained by propidium iodide (data not shown). No fluorescence was detected inside cells with FITC, SuperFect™, or FITC–

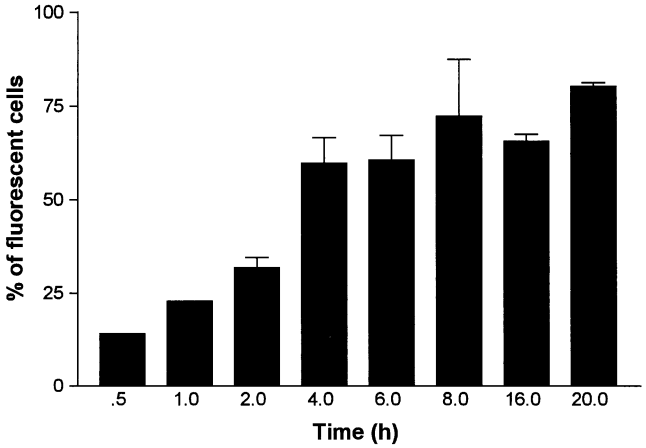

FIG. 2. Kinetics of the uptake of vectorized FITC–ODN. The percentage of fluorescent HeLa cells was determined by flow cytometry as a function of the time of incubation with FITC–ODN complexed to SuperFect™.

ODN alone. FITC alone complexed to SuperFect™ penetrated cells, but the fluorescence distribution exhibited was completely different from that observed with FITC–ODN. In fact, on incubation with FITC alone, cellular fluorescence was not localized in the nucleus or in vesicles, but was diffusely distributed in cells. Moreover, no significant ODN degradation was observed when FITC–ODN, complexed to SuperFect™, was extracted from HeLa cells after 16 hr of incubation and analyzed by PAGE (data not shown). Consequently, the fluorescence observed inside cells did not correspond to FITC alone or to degraded FITC–ODN but rather to intact FITC–ODN.

Influence of Cell Cycle Phase on Intracellular Distribution

A study of the cellular uptake and intracellular distribution of FITC–ODN as a function of the cell cycle phase could provide relevant information to explain the differences observed in the fluorescent cell population by flow cytometry and confocal microscopy. Hoechst staining was used to determine the phase of the cell cycle by flow cytometry. When the distribution in each phase of the cell cycle of the subpopulation of intensely fluorescent cells (Fig. 1, B′) was compared to that of all fluorescent cells, an increase in the percentage of cells in the G2/M phase and a decrease in the G1 phase were observed (Fig. 5). The increased proportion of intensely fluorescent cells in the G2/M phase was found at all times of FITC–ODN incubation tested (Table 2), and was reproducible from one experiment to another. Furthermore, for all fluorescent cells, the intensity of fluorescence was determined for each phase of the cell cycle and was found to be greater for cells in G2/M phase compared to those in the S and G1 phases (Table 3). Moreover, the addition of the ODN/SuperFect™ complex to cells did not change their cell cycle distribution (data not shown).

In addition, confocal microscopy analysis showed that dividing fluorescent cells always exhibited stronger nuclear

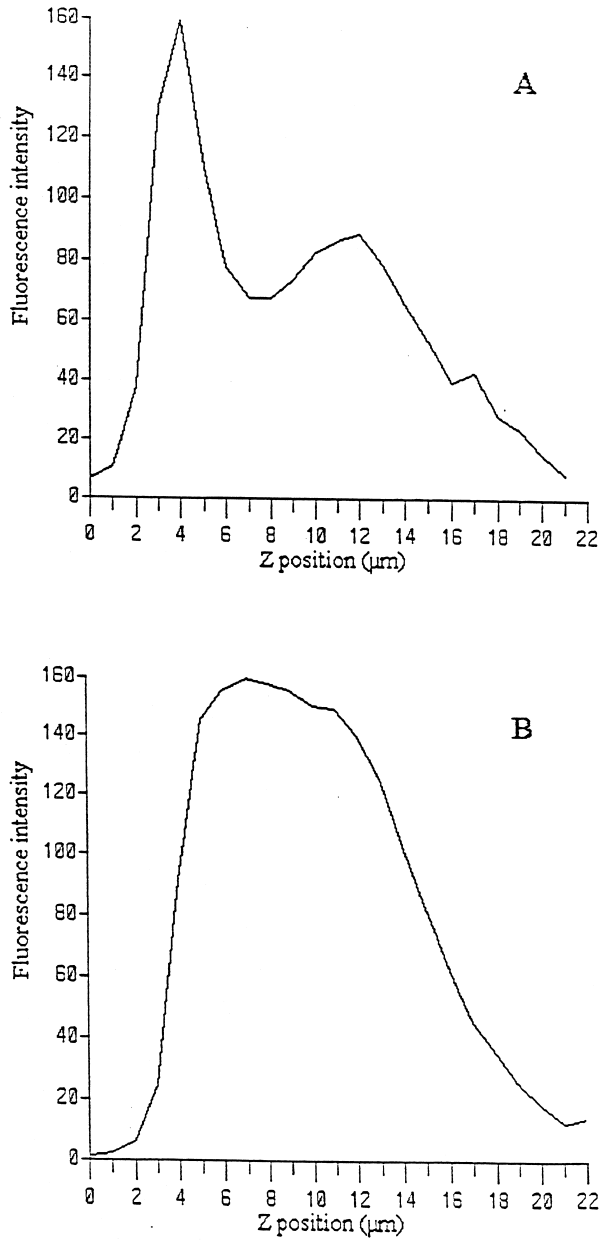

FIG. 3. Localization of FITC–ODN fluorescence in cells. HeLa cells were incubated for 1 hr (A) and 16 hr (B) with FITC–ODN complexed to SuperFect™, and the localization of FITC–ODN was determined by scanning with a laser confocal microscope at 1 μm increments in the Z-axis from the upper surface to the bottom of the cells (pinhole 400, range of 40–1600). Curves A and B show the relative fluorescence intensity as a function of the position on the Z-axis (cell membrane, from 0 to 3 μm and from 17 to 20 μm; inside of cell, from 3 to 17 μm).

fluorescence (Fig. 6). Considering the results obtained by flow cytometry, the strong intensity of fluorescence of cells in G2/M could then correspond to a nuclear FITC–ODN localization. Consequently, the variations in cellular fluorescence intensity dependent on the phase of the cell cycle could suggest a difference in intracellular distribution. To study this phenomenon in depth, HeLa cells were synchronized with a double thymidine block, and the intracellular

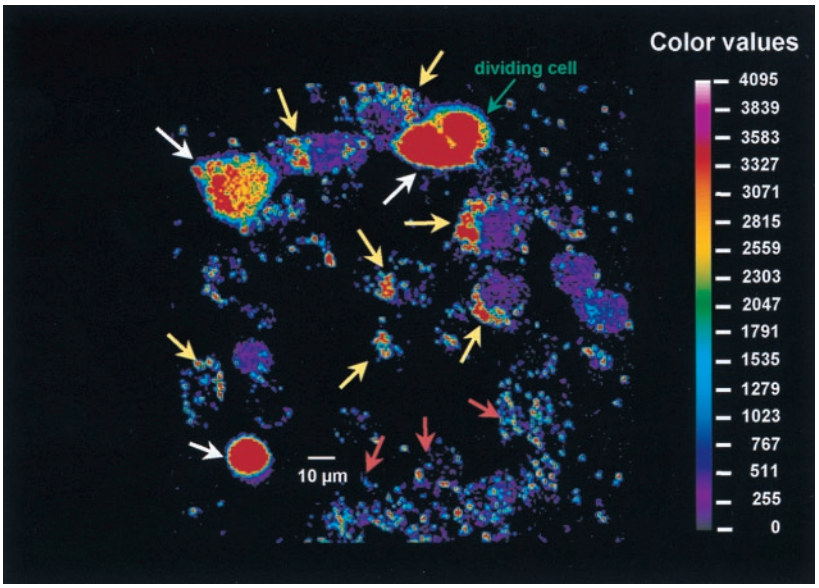

FIG. 4. Heterogeneous intracellular distribution of FITC–ODN (perinuclear and nuclear). HeLa cells were incubated for 16 hr with FITC–ODN complexed to SuperFect™ and analyzed with a laser confocal microscope (pinhole 400, range of 40–1600). The photograph is a two-dimensional non-confocal image showing cells with a perinuclear fluorescence (yellow arrows), a strong nuclear fluorescence (white arrows), and a cell surface fluorescence (red arrows). For some cells, the nuclear fluorescence is so great that it diffuses to the cytoplasm.

distribution of FITC–ODN was investigated by confocal microscopy after 4 hr of incubation with cells (the phase of the cell cycle was determined before confocal analysis by flow cytometry in cells treated in exactly the same way). Cells in the G2/M phase mainly exhibited nuclear fluorescence (Fig. 7), whereas cells in the G1 and S phases presented a heterogeneous distribution of fluorescence. When flow cytometry and confocal microscopy results were compared, the intensity of fluorescence appeared to be closely correlated with the FITC–ODN intracellular distribution and dependent on the phase of the cell cycle. When FITC–ODN was localized in the cell nucleus (G2/M phase), the intensity of fluorescence was higher than when it was localized in punctuated perinuclear vesicles.

Biological Activity of Vectorized ODNs

PROTEIN EXPRESSION. As shown above, the dendrimeric structure promoted FITC–ODN uptake in different cell lines. The antisense effect of vectorized ODNs was studied using two plasmids coding for two different reporter genes (β-gal and GFP). The reporter genes were under the control of the same promoter to avoid possible bias resulting from an ODN interaction with the promoter region. Four antisense ODNs were targeted on the initiation codon (AUG-ODNs) or an internal coding region (IN-ODNs) of each of the reporter genes (Table 1). A double mismatch, a scramble, and a reverse sequence of one of the antisense ODNs were tested as controls for antisense sequence specificity (Table 1). In order to enhance ODN resistance to nucleases, two phosphorothioate groups were introduced at both the 3′ and the 5′ ends. The plasmids were co-transfected simultaneously into HeLa cells using SuperFect™. The ODN complexed with the same transfecting reagent was added to cells 2 hr before the plasmids. β-gal and GFP expression was measured in the cell lysate, 16 hr after plasmid co-transfection. The ratio between protein activities (R_C) was determined using an ODN that was not complementary to either plasmid (Table 1) to eliminate possible variations in gene expression due to a polyanionic effect caused by any short nucleic acid sequence. To evaluate the inhibitory effect of the ODNs, the ratio between protein activities was measured in the presence of each ODN (R_{ODN}). The ratio between the above-described ratios (R_{ODN}/R_C) allowed us to determine the inhibitory activity of ODN. Thus, the non-targeted gene served as an internal control for cytotoxic effects and non-sequence specificity of the ODNs. No inhibition was observed when the ODNs were not vectorized (data not shown). The ODNs complexed to SuperFect™ exhibited a high inhibitory efficiency (76% of GFP inhibition with 5 μg of IN-GFP antisense). The ODNs targeting an internal coding region of each gene (IN-ODNs) were more efficient that those targeting the initiation codon (AUG-ODNs). When 5 μg of ODNs was complexed to SuperFect™, the inhibition of their respective targets obtained with IN-β-gal and IN-GFP ODNs was 54% and 76%, respectively, and only 16% and 49% with AUG-β-gal and AUG-GFP ODNs (SE ≅ 8%). Different quantities of the ODN giving the best result (IN-GFP antisense) were therefore complexed to SuperFect™ and tested (Fig. 8). The biological effect increased with the amount of ODN, and the dose-dependent curve reached a plateau at approximately 75% inhibition. Reverse and scramble ODNs presented a very weak effect compared to the antisense ODN, and the inhibition measured with the mismatch ODN (which contains 2 mismatches for 18 bases) reached a maximum of 34%. Under the biological assay conditions, the cytotoxicity of the ODN-SuperFect™ complex on HeLa cells was not greater than 10%.

MRNA EXPRESSION. The observed inhibition of GFP expression by IN-GFP antisense ODN was a sequence-specific effect but did not permit us to pinpoint the

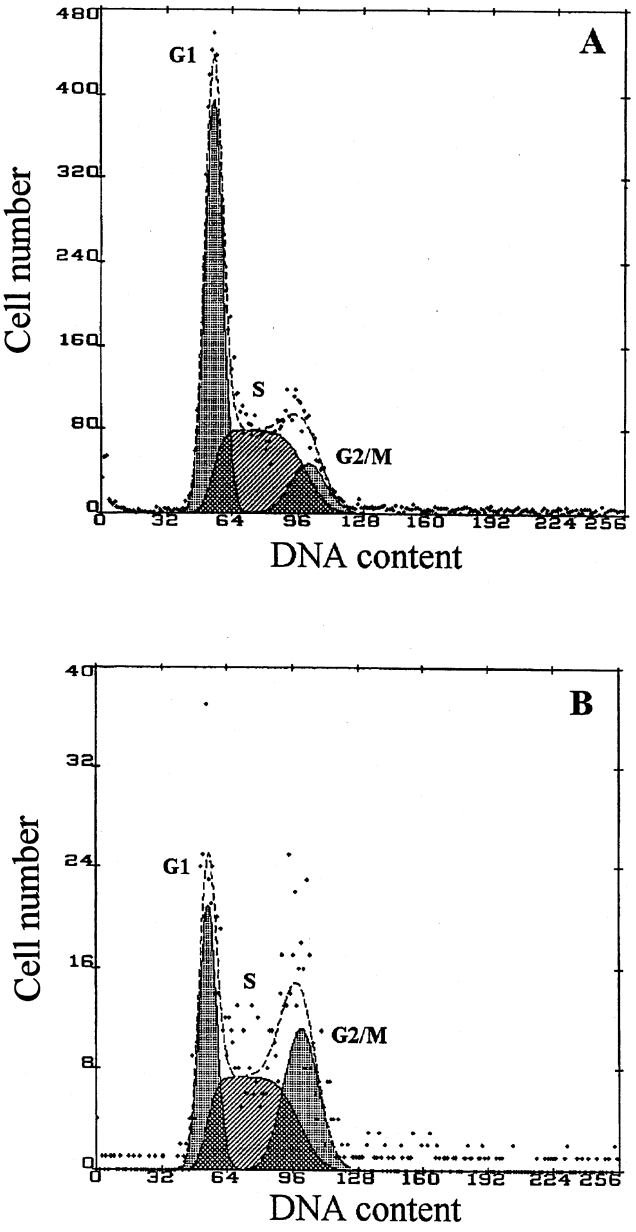

FIG. 5. Two different cell cycle patterns in the fluorescent cell population. (A) All fluorescent cells and (B) cells presenting a very high intensity of fluorescence (Fig. 1, B′). HeLa cells were incubated for 16 hr with the FITC–ODN–SuperFect™ complex. The different phases of the cell cycle were determined by flow cytometry after Hoechst staining using the Multicycle AV program.

mechanism of ODN action. Total cellular RNA was therefore analyzed for the presence of GFP mRNA by Northern blot hybridization in cells transfected with ODN and plasmids. On blots hybridized with the GFP probe, RNA from cells treated with control or scramble ODNs (Table 1) migrated as a single 1 kb band, whereas two bands (around 0.6 and 0.3 kb) appeared with IN-GFP antisense ODN. Figure 9 showed mRNA expression for different amounts of antisense ODN, and the two bands of 0.6 and 0.3 kb appeared clearly from 3 μg of ODN. The bands corresponding to β-actin showed that RNA loading and transfer were approximately the same for each band.

DISCUSSION

ODNs are capable of inhibiting or modulating the expression of target genes by an antisense mechanism or by other mechanisms such as triplex formation or decoy, but their activity is in part dependent on their ability to enter cells. After penetration, ODNs must also escape lysosomal degradation and proceed to interact with their RNA target. Membrane proteins interacting with ODN have been reported [42, 43], but these receptors are not always sufficient to ensure the biological efficiency of ODNs, especially in cell cultures. Consequently, carriers providing improved ODN transport into cells deserve persistent attention [5]. Among the eligible candidates likely to enhance ODN efficiency, we have studied the effects of a dendrimeric structure (SuperFect™) on the cellular uptake, intracellular distribution, and biological activity of ODNs.

It has already been described that phosphodiester ODNs labeled with an FITC group are protected in cells [34, 44]; here, we found that FITC–ODN complexed to SuperFect™ was not degraded inside cells. Consequently, the fluorescence observed during the different analyses corresponds to intact FITC–ODN. The fluorescence analysis performed in this study showed that non-vectorized ODNs were not detected in the different cell lines used. This suggests weak ODN uptake or even the complete absence of uptake. In contrast, vectorized ODNs were found inside cells, and the differences observed in uptake were dependent on the cell line. The best results were obtained on adherent cell lines (HeLa and NIH 3T3) (Fig. 1), where FITC–ODN uptake was rapid and plateaued after 4 hr of incubation (Fig. 2). Confocal microscopy analysis showed that some cells exhibited a perinuclear punctuated fluorescence while others showed obvious nuclear fluorescence (Fig. 4). These two typical patterns of cell fluorescence have also been reported with another dendrimeric structure and lipofectin [35]. When a kinetic study was performed by confocal microscopy, both types of fluorescence were observed whatever the duration of FITC–ODN incubation with cells or the time elapsed after removal of the medium with FITC–ODN. This result suggests that nuclear accumulation is not time-dependent, contrasting with results previously described for other ODN carriers [27, 28]. The flow cytometry analysis showed that some cells exhibited intense fluorescence (Fig. 1). These highly fluorescent cells presented a greater percentage of cells in G2/M, whereas the number of cells in G1 was lower when compared to the whole population of fluorescent cells (Table 2). Another important parameter is the sensitivity of FITC–ODN fluorescence to the acidity of the environment [45]. Vectorized FITC–ODN may, in fact, exhibit less intense fluorescence in vesicles with a low pH than when localized in a compartment, such as the nucleus, with a higher pH. The different fluorescence intensities of cells in each phase of

TABLE 2. Comparison of the distribution of fluorescent cells in each phase of the cell cycle

	Total fluorescent cells† (B + B′ in Fig. 1)			Subpopulation of cells exhibiting a strong intensity of fluorescence† (B′ in Fig. 1)		
Time* (hr)	GI	S (%)	G2/M	G1	S (%)	G2/M
2	43.0	36.7	20.3	34.3	32.0	33.7
6	36.9	42.8	20.3	37.6	29.3	33.1
8	41.2	36.9	21.8	36.2	28.4	35.4
16	53.2	43.6	3.2	47.2	39.9	12.9
20	52.9	39.1	8.0	43.7	36.6	19.7
24	41.7	43.5	14.8	33.8	40.2	26.0
mean ± SEM	44.8 ± 5.5	40.4 ± 2.9	14.7 ± 6.1	38.8 ± 4.4	34.4 ± 4.5	26.8 ± 7.3

*HeLa cells were incubated for different times with FITC–ODN complexed to SuperFect™; cell cycle measurements were performed by flow cytometry after Hoechst staining.

†The distribution of cells in each phase of the cell cycle is compared between the total fluorescent cell population (B + B′, Fig. 1) and the subpopulation of intensely fluorescent cells (B′, Fig. 1); the % of cells in G2/M is greater for intensely fluorescent cells whatever the time of FITC–ODN incubation.

the cell cycle (Table 3) might therefore be reflecting differences in intracellular compartmentalization of FITC–ODN. In addition, if the various sites of fluorescence observed by confocal microscopy are taken into account: i) the majority of FITC–ODN in G1 and S phases might have been localized inside endosomes or any other vesicle with an acid environment (Fig. 4) and ii) the increased intensity of fluorescence in the G2/M phase might have been due to localization in the nucleus. (Fig. 7). Alterations in the nuclear membrane during mitosis may facilitate FITC–ODN penetration into the nucleus. Therefore, two hypotheses can be formulated: i) the phase of the cell when the ODN is delivered is the significant factor for its localization, and there is no intracellular redistribution; and ii) the apparent stationary level of the intracellular distribution with time is the result of a nuclear accumulation when cells go through the G2/M phase followed by a cytoplasmic redistribution of ODNs. The different observations we made show the influence of cell cycle phase on the intracellular distribution of vectorized ODN, as previously reported regarding the uptake of free ODN [46, 47]. Moreover, this confirms the relevance of targeting rapidly dividing cells with antisense ODNs [48, 49]. Localization of ODN in the nucleus could be facilitated and thus permit the activation of RNase H-mediated degradation of the targeted RNA [50, 51]. We also noted that the intensity of fluorescence was higher for cells in the S phase compared to cells in G1, which could reveal a modification of the FITC–ODN environment at the G1/S transition.

The biological effect of ODNs complexed to the dendrimer vector was also studied. A rapid screening system allowing us to test compounds likely to enhance antisense ODN effects was developed. Two different reporter genes coding for readily measurable proteins, under the control of the same promoter, were used. Biological ODN activity was determined for one gene using the other gene as an internal control of ODN specificity. In addition, a non-complementary ODN was used as a control of transfection and gene expression. To limit the potential non-sequence-specific effects of phosphorothioate ODNs [12] and to enhance phosphodiester ODN resistance to nucleases, antisense activity was evaluated using chimeric ODNs containing only four phosphorothioate groups, two at each end. 18-mer ODNs complementary to the initiation codon (AUG-ODNs) and to an internal coding region (IN-ODNs) of the reporter genes were tested (Table 1). The ODNs targeting an internal region were found to be more effective. These results confirm that the initiation codon is not always the best target [5, 52]. Furthermore, the IN-ODN against the GFP reporter gene appeared to be more active than the IN-ODN against the β-gal plasmid. This might reflect different degrees of accessibility of targeted sites in mRNAs,

TABLE 3. Fluorescence intensity of non-synchronous (I) and synchronous (II) HeLa cells in each phase of the cell cycle

I				II	
	Cells in G1	Cells in S	Cells in G2	Cell cycle phase	Mean fluorescence
Non-synchronized cells*					
% of cells	48%	37%	15%	Cells in S phase*†	4.95
Mean fluorescence	3.62	4.63	5.66	Cells in G2/M phase*†	6.34
Cells accumulated in G1 phase*†					
% of cells	64%	15%	21%		
Mean fluorescence	4.31	5.71	9.26		

*HeLa cells were incubated for 4 hr with FITC–ODN complexed to SuperFect™; mean fluorescence of cells in each phase of the cell cycle was determined by flow cytometry after Hoechst staining.

†HeLa cells were treated with a double thymidine block, and cell cycle measurements were performed at different times after release from the double block.

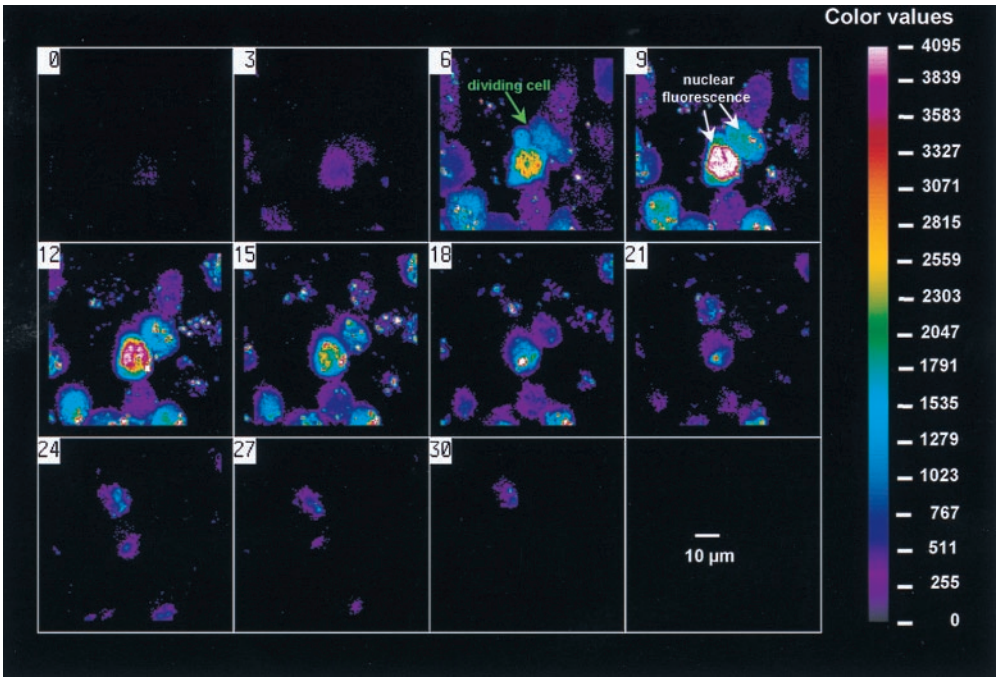

FIG. 6. Nuclear localization of FITC–ODN inside a cell in mitosis. HeLa cells were incubated for 16 hr with FITC–ODN complexed to SuperFect™ and analyzed with a laser confocal microscope (pinhole 400, range of 40–1600). The figure is a matrix of 12 optical sections of a dividing cell scanned at 1-µm increments along the Z-axis of cells (pseudo-color representation: black = lower fluorescence < blue < green < yellow < red = higher fluorescence). The number in the upper left corner is the position of the section in the Z-axis.

a parameter which is very important yet difficult to predict before cell experiments. The dependence of GFP expression on the quantity of IN-ODN reached a plateau (Fig. 8), and the various charge ratios of the complex could account for this. Indeed, the dose of the transfecting reagent remains constant as the ODN dose increases, and excess negative charges are then able to diminish uptake efficiency [28, 35]. A GFP sequence-specific inhibition of 76% was found with 5 µg of a chimeric ODN complexed to SuperFect™. In addition, the data obtained with the control ODNs (scramble, reverse, and mismatch) support the sequence specificity of the antisense effects observed (Fig. 8). The inhibition measured with the mismatch ODN can be explained by the fact that its sequence differs from the antisense ODN by only two bases (Table 1). In addition, mRNA analysis was carried out to study the mechanism of action of the efficient ODN in our screening assay system. The two bands observed with IN-GFP antisense are fully consistent with an RNase H-induced cleavage of the GFP mRNA (Fig. 9). In fact, the expected size of the GFP mRNA is around 1 kb and IN-GFP antisense targets the 1198–1215 position in the coding region. Consequently, after cleavage by RNase H, two fragments of GFP mRNA of 0.6 and 0.4 kb should be created. The second band was lower than expected (0.3 instead of 0.4 kb) but indeed corresponds to the strand with a 3′ end free likely shortened by 3′-exonucleases known to be very active in cells [27]. Consequently, this result is clear proof of an antisense

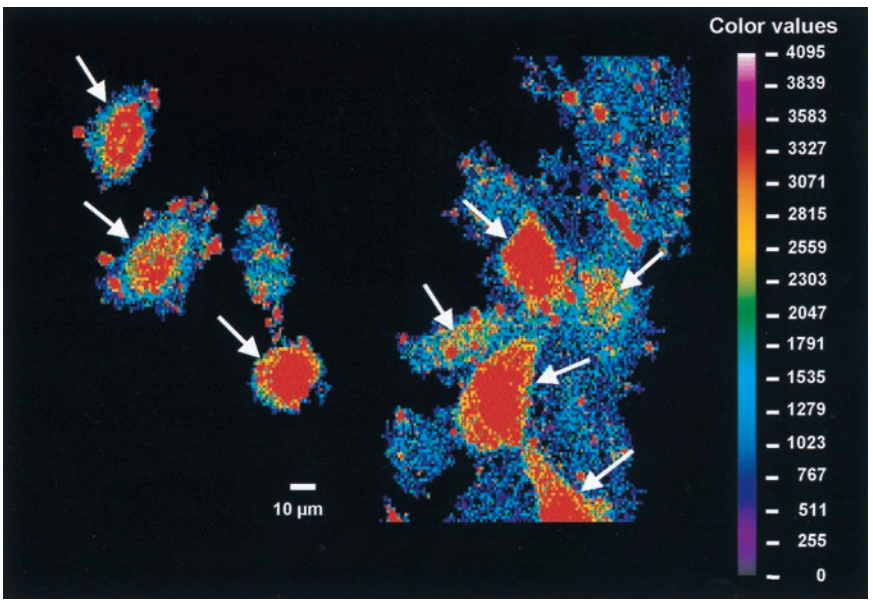

FIG. 7. Nuclear localization of FITC–ODN in cells in G2/M phase. HeLa cells synchronized in G2/M were incubated 4 h with the FITC–ODN–SuperFect™ complex and analysed with a laser confocal microscope. The photograph is a 2-dimensional non-confocal image. The nuclear fluorescence is outlined by white arrows (in some cells the intensity is so great that it diffuses to the cytoplasm).

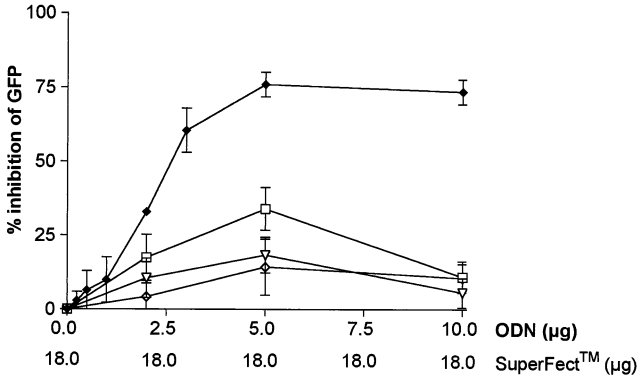

FIG. 8. Inhibition of GFP expression by vectorized ODNs. Different quantities of IN-GFP ODNs (antisense and controls) were complexed to SuperFect™ and incubated for 16 hr with HeLa cells co-transfected with GFP and β-gal plasmids. The percentage of inhibition was calculated as indicated in the text. The IN-GFP antisense (◆) and the IN-GFP controls (double mismatch [□], reverse [▽, and scramble [◇]) were added to cells 2 hr before the plasmid co-transfection.

mechanism and the screening system we have described appears to allow for the study of the biological activity and specificity of various modified antisense ODNs and ODN carriers.

In conclusion, we found that a dendrimeric structure permits efficient vectorization of ODNs, giving an antisense sequence-specific inhibition in the screening system we developed. Moreover, our study confirms that flow cytometry and confocal microscopy analyses are powerful tools with which antisense ODN delivery and efficiency can be optimized [34, 43, 53]. With the dendrimer vector, the intracellular distribution of ODNs is cell cycle-dependent, with nuclear localization facilitated in the G2/M phase. Thus, if the nucleus were a privileged site for ODN action—for example via an RNase H-dependent mechanism [54]—this result would have significance for the treatment of rapidly dividing cells.

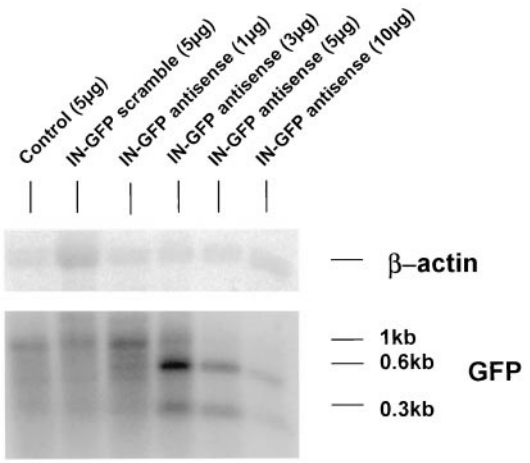

FIG. 9. Effect of vectorized ODNs on GFP mRNA. HeLa cells were treated with different amounts of ODNs complexed to SuperFect™ and co-transfected with plasmids. Sixteen hours after co-transfection, cells were lysed and analyzed for transcription of GFP and β-actin genes.

The authors wish to thank S. Kuznetsova, A. Debin, F. Svinarchuk, J. R. Bertrand and A. Maksimenko for helpful discussions and technical assistance. This work was supported by a grant (6317) from the Association pour la Recherche contre le Cancer (ARC), by the Centre National de la Recherche Scientifique (CNRS) and the ARC (jumelage Franco-Russe), and by the Russian Foundation for Basic Science (Grant 98-04-22055). M. L. received a fellowship from the ARC and V. H. is supported by the CNRS (Bourse Doctorat Ingenieur) and by the Institut de Formation Supérieure Biomédicale (IFSBM). The authors are grateful to L. Saint Ange for the linguistic revision of the manuscript and L. Pritchard for critical re-reading.

References

1. Akhtar S and Agrawal S, *In vivo* studies with antisense oligonucleotides. *Trends Pharmacol Sci* **18:** 12–18, 1997.
2. Bennett CF, Antisense oligonucleotides: Is the glass half full or half empty? *Biochem Pharmacol* **55:** 9–19, 1998.
3. Skorski T, Nieborowska-Skorska M, Barletta C, Malaguarnera L, Szcyzlik C, Chen ST, Lange B and Calabretta B, Highly efficient elimination of Philadelphia leukemic cells by exposure to bcr/abl antisense oligodeoxynucleotides combined with mafosfamide. *J Clin Invest* **92:** 194–202, 1993.
4. Bishop MR, Iversen PL, Bayever E, Sharp JG, Greiner TC, Copple BL, Ruddon R, Zon G, Spinolo J, Anerson M, Armitage JO and Kessinger A, Phase I trial of an antisense oligonucleotide OL(1)p53 in hematologic malignancies. *J Clin Oncol* **14:** 1320–1326, 1996.
5. Monia PB, Johnston JF, Geiger T, Muller M and Fabbro D, Antitumor activity of a phosphorothioate antisense oligodeoxynucleotide targeted against C-*raf* kinase. *Nat Med* **2:** 668–675, 1996.
6. Offensperger WB, Offensperger S, Walter E, Teubner K, Igloi G, Blum HE and Gerok W, *In vivo* inhibition of duck hepatitis B virus replication and gene expression by phosphorothioate-modified antisense oligodeoxynucleotides. *EMBO J* **12:** 1257–1262, 1993.
7. Lisziewicz J, Sun D, Weichold FF, Thierry AR, Lusso P, Tang J, Gallo RC and Agrawal S, Antisense oligodeoxynucleotide phosphorothioate complementary to Gag mRNA blocks replication of human immunodeficiency virus type 1 in human peripheral blood cells. *Proc Natl Acad Sci USA* **91:** 7942–7946, 1994.
8. Azad RF, Brown-Driver V, Buckheit RW and Anderson KP, Antiviral activity of a phophorothioate oligonucleotide complementary to human cytomegalovirus RNA when used in combination with antiviral nucleoside analogs. *Antivir Res* **28:** 101–111, 1995.
9. Uhlmann E and Peyman A, Antisense oligonucleotides: A new therapeutic principle. *Chem Rev* **90:** 544–584, 1990.
10. Gray GD, Basu S and Wickstrom E, Transformed and immortalized cellular uptake of oligodeoxynucleoside phosphorothioates, 3′-alkylamino oligodeoxynucleotides, 2′-*O*-methyl oligoribonucleotides, oligodeoxynucleoside methylphosphonates, and peptide nucleic acids. *Biochem Pharmacol* **53:** 1465–1476, 1997.
11. Wagner RW, Matteucci MD, Lewis JG, Gutierrez AJ, Moulds C and Froehler BC, Antisense gene inhibition by oligonucleotides containing C-5 propyne pyrimidines. *Science* **260:** 1510–1513, 1993.
12. Stein CA, Tonkinson JL and Yakubov L, Phosphorothioate oligodeoxynucleotides-antisense inhibitors of gene expression? *Pharmacol Ther* **52:** 365–384, 1991.

13. Boutorin AS, Gus'kova LV, Ivanova EM, Kobetz ND, Zarytova VF, Ryte AS, Yurchenko LV and Vlassov VV, Synthesis of alkylating oligonucleotide derivatives containing cholesterol or phenazinium residues at their 3′-terminus and their interaction with DNA within mammalian cells. *FEBS Lett* **254:** 129–132, 1989.
14. Boutorine AS and Kostina EV, Reversible covalent attachment of cholesterol to oligodeoxyribonucleotides for studies of the mechanisms of their penetration into eucaryotic cells. *Biochimie* **75:** 35–41, 1993.
15. Krieg AM, Tonkinson J, Matson S, Zhao Q, Saxon M, Zhang LM, Bhanja U, Yakubov L and Stein CA, Modification of antisense phosphodiester oligodeoxynucleotides by a 5′ cholesteryl moiety increases cellular association and improves efficacy. *Proc Natl Acad Sci USA* **90:** 1048–1052, 1993.
16. Asseline U, Hau JF, Czernecki S, Le Diguarher T, Perlat MC, Valery JM and Thuong MT, Synthesis and physicochemical properties of oligonucleotides built with either alpha-L or beta-L nucleotide units and covalently linked to an acridine derivative. *Nucleic Acids Res* **19:** 4067–4074, 1991.
17. Bongartz JP, Aubertin AM, Milhaud PG and Lebleu B, Improved biological activity of antisense oligonucleotides conjugated to a fusogenic peptide. *Nucleic Acids Res* **22:** 4681–4688, 1994.
18. Morris MC, Vidal P, Chaloin L, Heitz F and Divita G, A new peptide vector for efficient delivery of oligonucleotides into mammalian cells. *Nucleic Acids Res* **25:** 2730–2736, 1997.
19. Akhtar S and Juliano RL, Liposome delivery of antisense oligonucleotides: Adsorption and efflux characteristics of phosphorothioate oligodeoxynucleotides. *J Control Release* **22:** 47–56, 1992.
20. Ropert C, Lavignon M, Dubernet C, Couvreur P and Malvy C, Oligonucleotides encapsulated in pH-sensitive liposomes are efficient toward Friend retrovirus. *Biochem Biophys Res Commun* **183:** 879–885, 1992.
21. Leonetti JP, Machy P, Degols G, Lebleu B and Lesserman L, Antibody-targeted liposomes containing oligodeoxyribonucleotides complementary to viral RNA selectively inhibit viral replication. *Proc Natl Acad Sci USA* **87:** 2448–2451, 1990.
22. Zelphati O, Imbach JL, Signoret N, Zon G, Rayner B and Leserman L, Antisense oligonucleotides in solution or encapsulated in immunoliposomes inhibit replication of HIV-1 by several different mechanisms. *Nucleic Acids Res* **22:** 4307–4314, 1994.
23. Chavany C, Saison-Behmoaras T, Le Doan T, Puiseux F, Couvreur P and Hélène C, Adsorption of oligonucleotides onto polyisohexylcyanoacrylate nanoparticles protects them against nucleases and increases their cellular uptake. *Pharmacol Res* **11:** 1370–1378, 1994.
24. Schwab G, Chavany C, Duroux I, Goubin G, Lebeau J, Hélène C and Saison-Behmoaras T, Antisense oligonucleotides adsorbed to polyalkylcyanoacrylate nanoparticles specifically inhibit mutated Ha-*ras*-mediated cell proliferation and tumorigenicity in nude mice. *Proc Natl Acad Sci USA* **91:** 10460–10464, 1994.
25. Degols G, Leonetti JP, Benkirane M, Devaux C and Lebleu B, Poly(L-lysine)-conjugated oligonucleotides promote sequence-specific inhibition of acute HIV-1 infection. *Antisense Res Dev* **2:** 293–301, 1992.
26. Bennett CF, Chiang MY, Chan H, Shomaker JE and Mirabelli CK, Cationic lipids enhance cellular uptake and activity of phosphorothioate antisense oligonucleotides. *Mol Pharmacol* **41:** 1023–1033, 1992.
27. Capaccioli S, Di Pasquale G, Mini E, Mazzei T and Quatrone A, Cationic lipids improve antisense oligonucleotide uptake and prevent degradation in cultured cells and in human serum. *Biochem Biophys Res Commun* **197:** 818–825, 1993.
28. Zelphati O and Szoka FC Jr, Intracellular distribution and mechanism of delivery of oligonucleotides mediated by cationic lipids. *Pharmacol Res* **13:** 1367–1372, 1996.
29. Lewis JG, Lin KY, Kothavale A, Flanagan WM, Matteucci MD, Deprince RB, Mook RA Jr, Hendren RW and Wagner RW, A serum-resistant cytofectin for cellular delivery of antisense oligodeoxynucleotides and plasmid DNA. *Proc Natl Acad Sci USA* **93:** 3176–3181, 1996.
30. Goldman CK, Soroceanu L, Smith N, Gillepsie GY, Shaw W, Burgess S, Bilbao G and Curiel DT, *In vitro* and *in vivo* gene delivery mediated by a synthetic polycationic amino polymer. *Nat Biotechnol* **15:** 462–466, 1997.
31. Mahato RI, Takemura S, Akamatsu K, Nishikawa M, Takakura Y and Hashida M, Physicochemical and disposition characteristics of antisense oligonucleotides complexed with glycosylated poly(L-lysine). *Biochem Pharmacol* **53:** 887–895, 1997.
32. Kukowska-Latallo JF, Bielinska AU, Johnson J, Spindler R, Tomalia DA and Baker JR Jr, Efficient transfer of genetic material into mammalian cells using Starburst polyamidoamine dendrimers. *Proc Natl Acad Sci USA* **93:** 4897–4902, 1996.
33. Tang MX, Redemann CT and Szoka FC Jr, *In vitro* gene delivery by degraded polyamidoamine dendrimers. *Bioconjugate Chem* **7:** 703–714, 1996.
34. Poxon SW, Mitchell PM, Liang E and Hughes JA, Dendrimer delivery of oligonucleotides. *Drug Deliv* **3:** 255–261, 1996.
35. Delong R, Stephenson K, Loftus T, Fisher M, Alahari S, Nolting A and Juliano RL, Characterization of complexes of oligonucleotides with polyamidoamine starburst dendrimer effects on intracellular delivery. *J Pharm Sci* **86:** 762–764, 1997.
36. Bielinska A, Kulowska-Latallo JF, Johnson J, Tomalia DA and Baker JR, Regulation of *in vitro* gene expression using antisense oligonucleotides or antisense expression plasmids transfected using starburst PAMAM dendrimers. *Nucleic Acids Res* **24:** 2176–2182, 1996.
37. Hughes JA, Aronsohn AI, Avrutskaya AV and Juliano RL, Evaluation of adjuvants that enhance the effectiveness of antisense oligodeoxynucleotides. *Pharm Res* **13:** 404–410, 1996.
38. Gregoire M, Hernandez-Verdun D and Bouteille M, Visualisation of chromatin distribution in living PTO cells by Hoechst 33342 fluorescent staining. *Exp Cell Res* **152:** 38–46, 1984.
39. Stein GS, Stein JL, Lian JB, Last TJ, Owen T and McCabe L, Synchronization of normal diploid and transformed mammalian cells. In: *Cell biology: A Laboratory Handbook*, (Ed. Celis J), pp. 282–287. Academic Press, New York, 1994.
40. Misteli T and Spector DL, Applications of the green fluorescent protein in cell biology and biotechnology. *Nat Biotechnol* **15:** 961–964, 1997.
41. Vistica DT, Skehan P, Scudiero D, Monks A, Pittman A and Boyd MR, Tetrazolium-based assays for cellular viability: A critical examination of selected parameters affecting formazan production. *Cancer Res* **51:** 2515–2520, 1991.
42. Loke SL, Stein CA, Zhang XH, Mori K, Nakanishi M, Subasinghe C, Cohen JS and Neckers LM, Characterization of oligonucleotide transport into living cells. *Proc Natl Acad Sci USA* **86:** 3474–3478, 1989.
43. Yakubov LA, Deeva EA, Zarytova VF, Ivanova EM, Ryte AS, Yurchenko LV and Vlassov VV, Mechanism of oligonucleotide uptake by cells: Involvement of specific receptors? *Proc Natl Acad Sci USA* **86:** 6454–6458, 1989.
44. Stein CA, Tonkinson JL, Zhang LM, Yakubov L, Gervasoni J, Taub R and Rotenberg SA, Dynamics of the internalization of phosphodiester oligodeoxynucleotides in HL60 cells. *Biochemistry* **32:** 4855–4861, 1993.

45. Tonkinson JL and Stein CA, Patterns of intracellular compartmentalization, trafficking and acidification of 5′-fluorescein-labeled phosphodiester and phosphorothioate oligodeoxynucleotides in HL60 cells. *Nucleic Acids Res* **22:** 4268–4275, 1994.
46. Wu-Pong S, Bard J, Huffman J and Jimerson J, Oligonucleotide biological activity: Relationship to the cell cycle and nuclear transport. *Biol Cell* **89:** 257–261, 1997.
47. Zamecnik P, Aghajanian J, Zamecnik M, Goodchild J and Witman G, Electron micrographic studies of transport of oligodeoxynucleotides across eukaryotic cell membranes. *Proc Natl Acad Sci USA* **91:** 3156–3160, 1994.
48. Zhao Q, Song X, Waldschmidt T, Fisher E and Krieg AM, Oligonucleotide uptake in human hematopoietic cells is increased in leukemia and is related to cellular activation. *Blood* **88:** 1788–1795, 1996.
49. Krieg AM, Gmelig-Meyling F, Gourley MF, Kisch WJ, Chrisey LA and Steinberg AD, Uptake of oligodeoxyribonucleotides by lymphoid cells is heterogeneous and inducible. *Antisense Res Dev* **1:** 161–171, 1991.
50. Giles RV, Ruddell CJ, Spiller DG, Green JA and Tidd DM, Single base discrimination for ribonuclease H-dependent antisense effects within intact human leukaemia cells. *Nucleic Acids Res* **23:** 954–961, 1995.
51. Moulds C, Lewis JG, Froehler BC, Grant D, Huang T, Milligan JF, Matteuci MD and Wagner RW, Site and mechanism of antisense inhibition by C-5 propyne oligonucleotides. *Biochemistry* **34:** 5044–5053, 1995.
52. Monia BP, Johnston JF, Ecker DJ, Zounes MA, Lima WF and Freier SM, Selective inhibition of mutant Ha-*ras* mRNA expression by antisense oligonucleotides. *J Biol Chem* **267:** 19954–19962, 1992.
53. Butler M, Stecker K and Bennett CF, Cellular distribution of phosphorothioate oligodeoxynucleotides in normal rodent tissues. *Lab Invest* **77:** 379–388, 1997.
54. Moulds C, Lewis JG, Froehler BC, Grant D, Huang T, Milligan JF, Matteucci MD and Wagner RW, Site and mechanism of antisense inhibition by C-5 propyne oligonucleotides. *Biochemistry* **34:** 5044–5053, 1995.